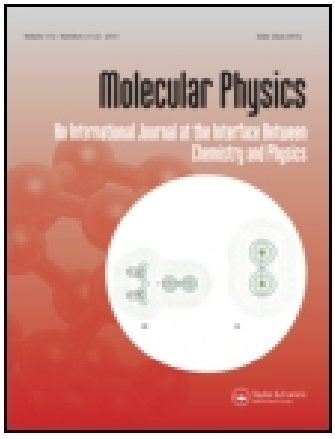

Molecular Physics: An International Journal at the Interface Between Chemistry and Physics
Publication details, including instructions for authors and subscription information:
http://www.tandfonline.com/loi/tmph20

Influence of microroughness on the wetting properties of nano-porous silica matrices

M. Śliwińska-Bartkowiak[a], A. Sterczyńska[ab], Y. Long[c] & K.E. Gubbins[d]
[a] Faculty of Physics, Adam Mickiewicz University, Poznan, Poland
[b] NanoBioMedical Centre, Adam Mickiewicz University, Poznan, Poland
[c] Department of Chemical & Biomolecular Engineering, National University of Singapore, Singapore
[d] Department of Chemical & Biomolecular Engineering, North Carolina State University, Raleigh, NC, USA
Published online: 18 Aug 2014.

To cite this article: M. Śliwińska-Bartkowiak, A. Sterczyńska, Y. Long & K.E. Gubbins (2014) Influence of microroughness on the wetting properties of nano-porous silica matrices, Molecular Physics: An International Journal at the Interface Between Chemistry and Physics, 112:17, 2365-2371, DOI: 10.1080/00268976.2014.935820

To link to this article: http://dx.doi.org/10.1080/00268976.2014.935820

Molecular Physics, 2014
Vol. 112, No. 17, 2365–2371, http://dx.doi.org/10.1080/00268976.2014.935820

INVITED ARTICLE

Influence of microroughness on the wetting properties of nano-porous silica matrices

M. Śliwińska-Bartkowiak[a], A. Sterczyńska[a,b], Y. Long[c] and K.E. Gubbins[d,*]

[a]*Faculty of Physics, Adam Mickiewicz University, Poznan, Poland;* [b]*NanoBioMedical Centre, Adam Mickiewicz University, Poznan, Poland;* [c]*Department of Chemical & Biomolecular Engineering, National University of Singapore, Singapore;* [d]*Department of Chemical & Biomolecular Engineering, North Carolina State University, Raleigh, NC, USA*

(*Received 12 February 2014; accepted 12 June 2014*)

We report experimental measurements of the contact angle for four liquids on four different silica substrates, the systems covering a wide range of wettabilities. One of the substrates is a smooth planar silica surface, while the others have rough surfaces and meso-pores. We discuss the measured contact angles in relations to the *microscopic wetting parameter*, α_w. This parameter emerges naturally from a corresponding states analysis of the partition function for this system, and is a measure of the ratio of the liquid–substrate intermolecular interaction to the interaction between two of the liquid molecules. Thus, it is a well-defined measure of wettability at both the nano- and macro-scales. The *microscopic wetting parameter* is shown to be a monotonic function of the contact angle. The contact angles for the materials with rough surfaces are found to be larger than those for the smooth planar surface for all liquids studied, including both non-wetting and wetting liquids. These results are discussed within the framework of a modified Cassie–Baxter model, in which only a fraction f of the liquid–solid interface is in actual contact with the solid. This fraction f is shown to increase as the wetting parameter increases in a physically reasonable way.

Keywords: wetting; nano-porous silica; contact angle; surface roughness

1. Introduction

At the macro-scale, it is usual to discuss the degree to which a liquid wets a solid surface in terms of the contact angle, θ_c, and its dependence on the surface tensions for the interfaces involved. For a smooth planar surface, these are related by a simple force balance, as stated by Young [1] (Figure 1):

$$\gamma_{SG} - \gamma_{SL} = \gamma_{LG} \cos\theta_c \tag{1}$$

In the case of liquid water, when the contact angle is less than 90°, the surface is usually referred to as hydrophilic ($\cos\theta_c > 0$) whereas for contact angles greater than 90°, the surface is hydrophobic ($\cos\theta_c < 0$). The difference in surface tensions, $\gamma_{SG} - \gamma_{SL} = A$, is the adhesion. A will be positive for a hydrophilic surface (wetting or spreading) and negative for a hydrophobic surface (resistance to wetting), and represents the energy per unit area needed to remove the liquid from the surface.

Most solid surfaces exhibit roughness, which may be on a macroscopic or microscopic scale, or there may be several relevant length scales [2]. Two models of roughness are often invoked, those of Wenzel [3] and of Cassie and Baxter [4], and are illustrated in Figure 2. In the Wenzel (W) model, the liquid is assumed to follow the irregularities in the solid surface, penetrating any cavities. The 'roughness factor', r, is defined as

$$r = \frac{\text{actual area of rough surface}}{\text{area of equivalent geometric surface}} \tag{2}$$

where the equivalent geometric surface is the smooth planar surface. Clearly, $r \geq 1$. In Wenzel's model, Equation (1) is replaced by $r\gamma_{SG} - r\gamma_{SL} = rA = \gamma_{LG}\cos\theta_c^W$, where θ_c^W is the apparent contact angle according to Wenzel. Comparison of this equation with Equation (1) gives

$$\cos\theta_c^W = r\cos\theta_c \tag{3}$$

where θ_c is the contact angle according to Young's equation (1). Since $r > 1$, in general, for $\theta_c < 90°$ ($\cos\theta_c > 0$), the Wenzel contact angle $\theta_c^W < \theta_c$, i.e. the rough surface is more hydrophilic than the smooth planar hydrophilic one, whereas if $\theta_c > 90°$ ($\cos\theta_c < 0$), the Wenzel contact angle $\theta_c^W > \theta_c$ and the rough surface is more hydrophobic than the smooth planar hydrophobic one. These effects will be enhanced by increasing the roughness factor, r. (Note that Equation (3) cannot hold in the limits $\theta_c \to 0°$ and $\theta_c \to 180°$, since $\cos\theta_c$ would take unphysical values.)

In the Cassie–Baxter (CB) model [4], the liquid does not penetrate into cavities, but sits on top of the 'posts' as shown in Figure 2, a condition sometimes referred to as the 'fakir

* Corresponding author. Email: keg@ncsu.edu

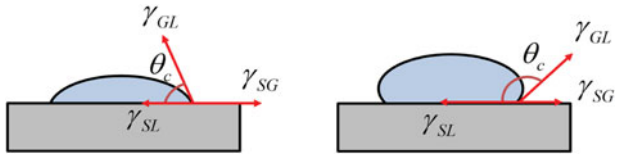

Figure 1. Wetting of a smooth planar solid surface by a liquid at the macro-scale, for strong wetting (hydrophilic case, left) and weak wetting or non-wetting (hydrophobic case, right). Arrows indicate the forces due to surface tensions for the solid (S), gas (G) and liquid (L) phases.

state' [5]. In this model, the apparent contact angle, θ_c^{CB}, is given by $\cos\theta_c^{\mathrm{CB}} = f\cos\theta_c + (1-f)\cos\theta_A$, where f is the surface fraction of the liquid that is in contact with the solid, $(1-f)$ is the surface fraction of liquid in contact with air between the 'posts', and θ_c and θ_A are the contact angles against the solid (Young's angle) and air, respectively. If we take the contact angle to be 180° for air, this becomes

$$\cos\theta_c^{\mathrm{CB}} = f(1+\cos\theta_c) - 1 \tag{4}$$

Thus, the smaller the fraction, f, of solid surface in contact with the liquid the more hydrophobic the surface will be, and in the limit $f \to 0$ the contact angle θ_c^{CB} will tend to 180°. Surfaces in which the apparent contact angle exceeds 150° are referred to as superamphiphobic (superhydrophobic in the case of water), and numerous examples of such surfaces occur in nature, in both the plant (the lotus leaf being the best known) and animal (the water strider and similar insects that walk on water) kingdoms [5–7]. In many of these naturally occurring surfaces, the superhydrophobicity arises from a CB mechanism, through achievement of a very small fraction of surface contact, f, between the surface and water.

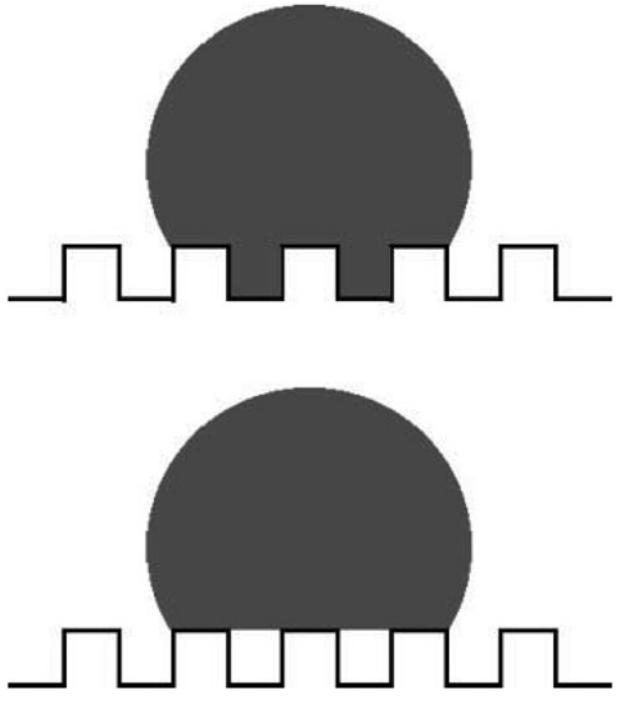

Figure 2. The Wenzel model, top, in which the liquid fully wets the rough surface, and the Cassie–Baxter model, bottom, in which the liquid does not penetrate the hollows, but sits on top of the 'posts'.

The Wenzel and Cassie–Baxter models cannot, in most cases, quantitatively describe the contact angle for real materials with rough surfaces. For example, intermediate behaviour between those exhibited in Figure 2 is likely, surfaces may be fractal and have roughness on several length scales, and the water–air surface in the CB model may be curved. However, the W and CB models provide a useful frame of reference for discussing the behaviour of real surfaces.

The above treatments are applicable to macroscopic and meso-scale systems. However, for sufficiently small nano-scale systems, for example a fluid wetting a nano-particle or the walls of a nano-pore, the surface tension concept breaks down because there is no longer a clearly defined interface separating two bulk phases [8]. Nevertheless, the degree to which a nano-phase 'likes' a solid substrate remains an important factor in determining the behaviour of such nano-scale systems, and it is useful to have a quantitative measure of this. The tendency of an adsorbate to wet a solid substrate is the result of a competition between the intermolecular forces between the adsorbate–substrate and the adsorbate–adsorbate interactions within the fluid itself. This is true whether the system is a nano-scale or macroscopic one. It is possible to derive a molecular level measure of wettability by carrying out a corresponding states analysis of the grand partition function for a simple model of a liquid in contact with a solid substrate, it being assumed that the intermolecular interactions can be described as effectively spherical using a universal function of separation distance and two adjustable parameters, ε (energy) and σ (length) [9,10]. The liquid–solid system is in equilibrium with a gas phase at temperature T and pressure P_{bulk}. For some dimensionless intensive property, b, for example the contact angle or the density, the corresponding states relation is [9]

$$b = b\left(P^*_{\mathrm{bulk}}, T^*;\ \alpha_w, \sigma_{as}/\sigma_{aa}\right) \tag{5}$$

where a and s represent adsorbate molecule and substrate atom, respectively, $P^*_{\mathrm{bulk}} = P_{\mathrm{bulk}}\sigma^3_{aa}/\varepsilon_{aa}$ and $T^* = kT/\varepsilon_{aa}$ are dimensionless bulk pressure and temperature, and α_w is a *microscopic wetting parameter* given by

$$\alpha_w = \rho_s\sigma^2_{as}\Delta(\varepsilon_{as}/\varepsilon_{aa}) \tag{6}$$

where ρ_s is the number of solid atoms per unit volume in the substrate and Δ is the distance separating layers of substrate atoms. The wetting parameter measures

the relative attractive strengths of the adsorbate–substrate and adsorbate–adsorbate interactions. For macroscopic systems, when $\alpha_w \to 0$ the contact angle $\theta_c \to 180^\circ$ (superamphiphobicity) while for very large values of α_w the contact angle will approach 0°. Molecular simulation studies [9] have shown that when the diameters σ_{aa} and σ_{as} are not very different, the size ratio, σ_{as}/σ_{aa}, has only a minor effect; in such cases, Equation (5) can be approximated by

$$b = b\left(P^*_{\text{bulk}}, T^*;\ \alpha_w\right) \tag{7}$$

Thus, the variable b depends on the two state variables, pressure and temperature, of the bulk gas phase, and one system variable, α_w.

In this paper, we report experimental measurements of the contact angle for several liquids on both rough (mesoporous) and smooth planar silica surfaces. We employ three types of porous silica, namely SBA-15, Al-SBA-15 and silica with 'ink-bottle' pores, having pore diameters in the range of 3.6–6.4 nm. 'Ink-bottle' pores consist of a cylindrical pore closed at one end, but open at the other through a narrow neck [11]. The results demonstrate the influence of roughness and the value of the *microscopic wetting parameter* in determining the contact angle. We discuss the results in terms of both the macroscopic classical wetting models and the *microscopic wetting parameter*.

2. Experimental method

2.1. Materials studied

We have studied the wetting behaviour for four liquids, water, heavy water, carbon tetrachloride and octamethylcyclotetrasiloxane (OMCTS), on both a planar smooth silica surface and on three nano-porous silica matrices, namely SBA-15, Al-SBA-15 and silica having ink-bottle pores [12]. In the case of the planar smooth silica surface, we have also measured the wetting behaviour of liquid mercury. Properties of the liquids studied are given in Table 1. The syntheses of Al-SBA-15 and SBA-15 followed a procedure that is a modification of the methods described by Bhange *et al.* [13] and Joo *et al.* [14], respectively. The SBA-15 material had a mean meso-pore diameter of 4.9 nm, while the Al-SBA-15 had a mean pore diameter of 4.6 nm and a molar ratio n(Si)/n(Al) equal to 80/1. The ink-bottle pores had a mean neck diameter of 3.6 nm and a cavity diameter of 6.4 nm. As the planar smooth silica material, the glass type 'KS-Kavalier' from Megan Poland was used, which contains about 80% of SiO_2, 11% of Na_2O and 9% of CaO.

Table 1. Liquid properties needed to calculate the contact angles.[a]

Fluid	Density (g cm^{-3})	Viscosity (mPa s)	Surface tension (mN m^{-1})
Water	0.9986	1.002	72.8
Heavy water	1.11	1.25	71.72
Carbon tetrachloride	1.584	0.901	27.0
OMCTS	0.96	2.45	18.50
Mercury	13.579	1.554	428
n-Heptane	0.682	0.6	20.14
n-Nonane	0.7177	0.714	22.62
n-Decane	0.7301	0.92	23.83

[a]All values are given at room temperature (295 K).

2.2. Contact angle measurements

The advancing contact angle was measured for both the smooth, planar silica material and for the porous silicas. For the smooth, planar silica surface, measurements were made with a SEO Phoenix 300 tensiometer using the sessile drop method. Fluid droplets are added until a plateau in the contact angle is reached. This plateau is known as the 'advancing contact angle'. The tensiometer allowed for drop shape measurements followed by analysis and calculation of contact angles and solid–liquid interfacial energies using the SEO Surfaceware7 version 1.0 software. Liquid drops were formed using a manual handle at the end of a syringe, and were then applied to the surface. By adjusting the backlight intensity, the camera–sample distance and the camera tilt angle, the selected part of the sample was observed. The tensiometer permitted the average value of the measured contact angles from the right and left sides of the droplet to be obtained. Contact angles were calculated based on Young's equation (1), with the standard values of the surface tensions of the liquids studied (Table 1).

The wetting of powders and porous solids also involves contact angle phenomena but is complicated by the presence of a porous architecture. The capillary rise method [15–18] presents the only method of contact angle measurement available for the measurement of tubular materials and coatings. Some strategies include binding the powder to a solid substrate and proceeding to measure contact angle on the sample produced. Interactions with the binding element (e.g. tape) and quantification of the amount bound introduce factors which may affect results. Temperature can be maintained in this method over a short period of time. This method is based on the measurement of the rate of liquid rise in the capillary with the porous fill. It is one of the most accurate methods for contact angle determination. The column of packed particles is assumed to behave like a bundle of capillaries where only laminar flow exists. Poiseuille's law describes the dependence between the rate of liquid rise and an increasing internal pressure due to this capillary rise:

$$dV = \frac{R^4 \Delta p \pi}{8\eta h} dt \tag{8}$$

where dV/dt is the volumetric flow rate of liquid penetration, R is the capillary radius, Δp is the pressure difference

across the curved surface of the liquid in the capillary, η is the viscosity of the penetrating liquid and h is the liquid rise in the capillary. The volume of liquid needed to raise the height of liquid by dh is $dV = (\pi R^2)dh$, so that Equation (8) can be written as

$$\frac{dh}{dt} = \frac{R^2}{8\eta h}\Delta p \tag{9}$$

The pressure difference between the capillary pressure and hydrostatic pressure is given by [19]

$$\Delta p = \frac{2\gamma \cos\theta_c}{R} - \Delta\rho g h \tag{10}$$

where $\gamma = \gamma_{LG}$ is the (liquid–gas) surface tension, θ_c is the advancing dynamic contact angle and $\Delta\rho$ is the density difference between the liquid and the surrounding medium (the porous bed). After substituting Equations (6) and (7) into Equation (1), we obtain the Washburn equation [15,20] for a vertical tube, in which the capillary rise is retarded by gravity. For capillaries with a small radius, the pressure increment due to the hydrostatic effect can be neglected, and we have the following dependence:

$$\frac{dh}{dt} = \frac{R\gamma \cos\theta_c}{4\eta h} \tag{11}$$

which, after integration, leads to the Washburn equation as

$$h^2 = \frac{R_{\text{eff}}\gamma \cos\theta_c}{2\eta}t \tag{12}$$

where R_{eff} is the effective capillary radius and is a particle-specific property. It depends on the kinds, shapes and diameters of sieves in the porous bed. We have calculated the dynamic advancing contact angles, θ_c, using the modified Washburn's equation:

$$m^2 = \frac{C\rho^2\gamma \cos\theta_c}{\eta}t \tag{13}$$

where m is the mass of liquid penetrating the porous fill in time t and ρ is the density of the wetting liquid. C is a constant for a given substrate, independent of the liquid but depending on the packing density of the molecular sieves and also on the pore size distribution.

A Sigma 700/701 tensiometer (Figure 3) was used to measure the contact angles in porous solids. It consisted of a sintered glass sample tube of diameter 3 mm, where the powders to be studied were placed, and a vessel of diameter 22 mm and maximum volume of 10 ml to contain the liquid. The latter is placed on a stage driven by a motor, and the sample tube, which is suspended from an electronic balance, is lowered into the liquid to the desired height at a low constant rate of 10 mm min^{-1}. The immersion depth

Figure 3. The tensiometer used to study porous solids.

into the liquid was equal to 1 mm. Before the experiment, the powders were dried in a vacuum dryer at 110 °C for 24 h. To obtain a uniform packing of the particles, the glass tube filled with the sample was vibrated for 60 s. During the experiment, the sample tube and the vessel containing the test liquids were kept at a temperature of 293 ± 0.5 K. The tensiometer was controlled by a computer software (KSV Co., Finland).

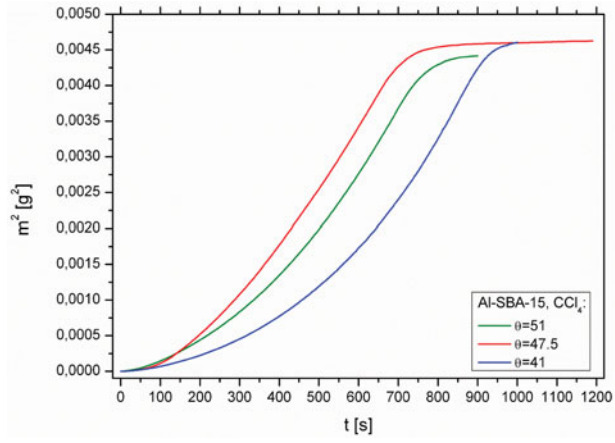

Figure 4. An experimental curve of m^2 vs. t for carbon tetrachloride penetrating the porous bed of Al-SBA-15.

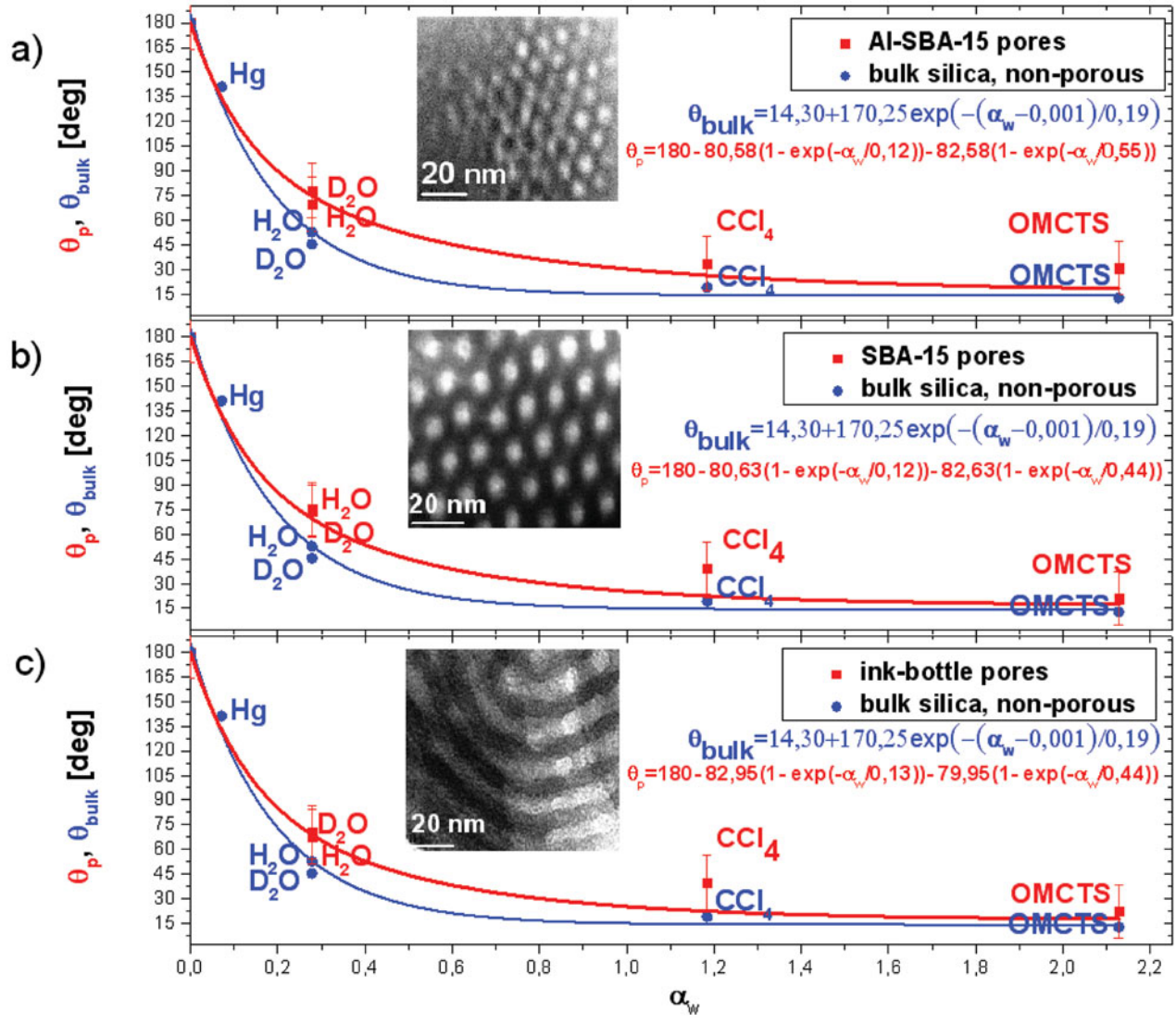

Figure 5. Experimentally measured contact angles for various liquids on the smooth planar silica surface (θ_{bulk}, lower blue points and curves) and on the rough meso-porous materials (θ_p, upper red points and curves): (a) Al-SBA-15; (b) silica SBA-15; (c) silica having ink-bottle pores. Transmission electron microscopy images provide some guidance as to the structure of the meso-porous materials. The curves are fits to the data using the exponential functions shown.

Table 2. Values of the contact angles and the fractions of liquid interface in contact with solid.

	Substrate							
	Glass (bulk)		Al-SBA-15		SBA-15		Ink-bottle	
Liquid	α_w	θ_c (°)	θ_c (°)	f	θ_c (°)	f	θ_c (°)	f
OMCTS	2.13	12.7	41.0	0.94	19.0	0.98	22.3	0.97
CCl_4	1.18	19.1	49.8	0.94	58.4	0.91	59.0	0.91
H_2O	0.28	52.8	63.7	0.84	68.8	0.78	57.8	0.86
D_2O	0.28	45.4	73.0	0.71	68.0	0.75	60.5	0.78

The experiment involved measuring the mass of the adsorbed liquid vs. time. From Equation (13), a graph of mass^2 vs. time should yield a straight line whose slope is $C\rho^2\gamma\cos\theta_c/\eta$. Since viscosity, density and surface tension are known (Table 1), there are only two unknowns left in this term, contact angle θ_c and the material constant for the solid, C. To resolve this situation, an experiment was performed for each of the porous solids using a liquid with very low surface tension, for which the contact angle can be assumed to be zero. In our experiment, *n*-heptane, *n*-nonane and *n*-decane were used. The material constant for the solid could then be obtained from the slope of m^2vs.t (slope $= C\rho^2\gamma/\eta$). For a particular solid, we assume that C is constant for various liquids, and then repeat the experiment for various liquids to determine the contact angles. An example of the curve for m^2 vs. t for carbon tetrachloride penetrating the porous bed of Al-SBA-15 (4.6 nm mesopore diameter) is shown in Figure 4. In our experiment, the reproducibility of the results was checked by three to five repetitions of the measurement, and then the average value of contact angle was obtained from the linear parts of the m^2vs.t curves. The measurement was stopped when this curve had reached saturation, which is manifested as a plateau (Figure 4).

3. Results and discussion

The measured contact angles are shown in Figure 5 and Table 2 as a function of the *microscopic wetting parameter*, α_w, for both the smooth planar silica surface and the three rough meso-porous materials. Values of α_w are for the liquids on a silica substrate, and are taken from the literature [9,10,21]. We estimate the accuracy of these measurements to be $\pm1^\circ$ for the planar silica surface, and approximately $\pm10^\circ$ for the rough meso-porous materials. We note the strong correlation between the macroscopic contact angle and the wetting parameter, as suggested by Equation (7). We do not expect the correlation to be perfect, since the reduced temperature will be somewhat different for the various liquids. However, molecular simulation results for the contact angle on geometrically rough surfaces [22] suggest that the influence of variation in reduced temperature on the contact angles will be relatively small for the range of reduced temperatures involved here. The rough meso-porous materials exhibit larger contact angles than those found for the smooth planar silica (Young's angle) for all values of the wetting parameter studied. The difference between the curves for the smooth and rough surfaces is the greatest for intermediate values of α_w. This is because the two curves must meet when $\alpha_w \to 0$ and $\alpha_w \to \infty$, since the contact angle cannot be smaller than 0° or larger than 180°. Thus the effect of roughness on the contact angle is greater for water and carbon tetrachloride than for OMCTS.

The results suggest a modified Cassie–Baxter mechanism, at least for smaller values of the wetting parameter.

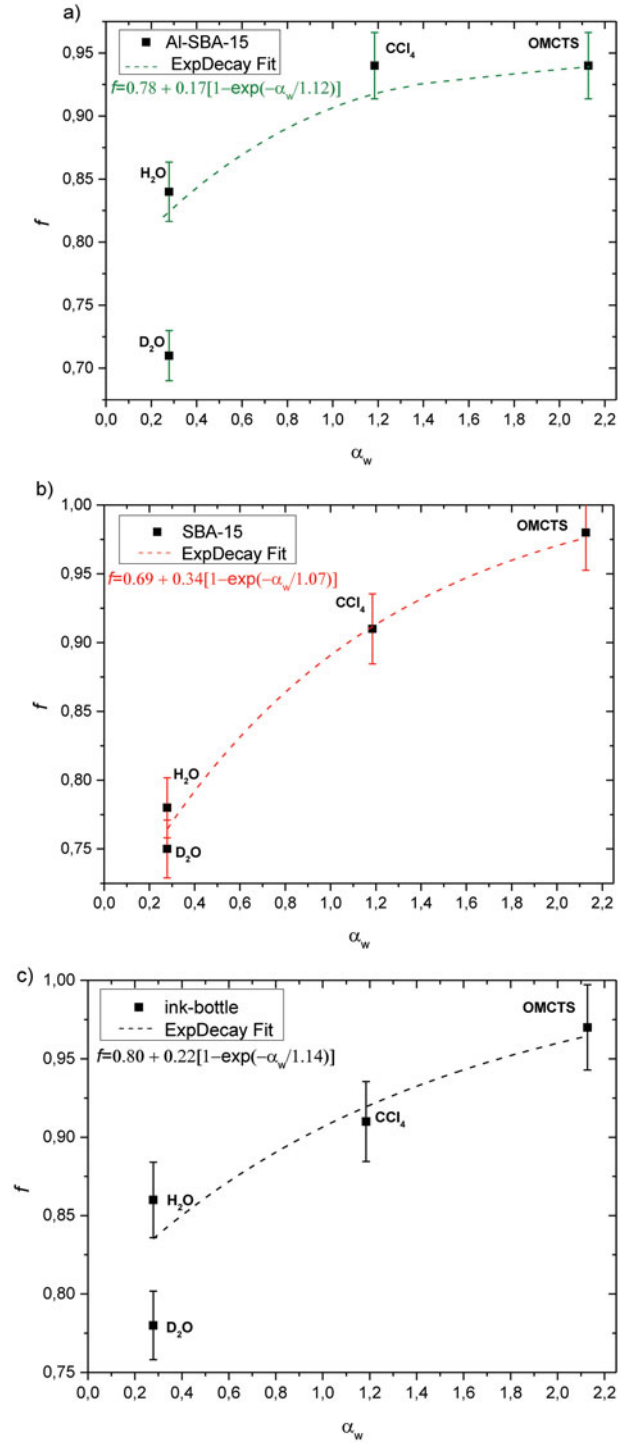

Figure 6. The fraction, f, of the liquid interface that is in contact with the solid substrate: (a) Al-SBA-15; (b) SBA-15; (c) ink-bottle pores. Points are calculated from Equation (4); curves are a guide for the eye.

For geometrically rough surfaces that are regular and whose roughness is on a single length scale (as in Figure 2), molecular simulation [22] and density functional theory [23] studies have shown that the wetting follows a Cassie–Baxter mechanism for small values of the *microscopic wetting parameter*, α_w, but at higher values there is a sharp transition to a Wenzel mechanism. For materials such as those studied here, however, we can expect roughness on several length scales, and some variation in the local value of the wetting parameter as an adsorbate molecule traverses the surface due to varied strength of adsorption sites. We can anticipate that for small values of α_w the liquid will not penetrate into the meso-pores under ambient conditions (as observed for mercury, for which $\alpha_w = 0.07$ on a silica surface, in laboratory measurements) but as α_w increases liquid will start to enter these pores and will penetrate other irregularities in the surface. If the wetting mechanism is a modified Cassie–Baxter one (Figure 2), we can expect the fraction, *f*, of the liquid interface that is in contact with the solid to increase as α_w increases. If we postulate such a CB mechanism, the fraction, *f*, is readily calculated from Equation (4) using the measured contact angles. The resulting fractions are shown in Figure 6. As expected, the fraction, *f*, increases as the wetting parameter increases, supporting the modified CB mechanism.

4. Conclusions

We have reported experimental measurements of the advancing contact angle for several liquids on both the smooth planar and rough meso-porous silica materials, and have shown that these measured values are closely correlated to the *microscopic wetting parameter*, α_w, which measures wettability in terms of the underlying intermolecular forces and is a valid measure at the nano-scale. The contact angle values for the rough meso-porous silicas are larger than those for the same liquid on the smooth planar silica surface for all the cases studied. By assuming that the wetting on the rough surfaces occurs by a modified Cassie–Baxter mechanism, in which only a fraction, *f*, of the liquid interface is in direct contact with the solid, we calculate this fraction and show that it possesses physically reasonable values, in the range of 0.72 (D_2O) to 0.96 (OMCTS). Moreover, the fraction, *f*, in contact with the solid substrate increases monotonically as the wetting parameter α_w increases, as might be expected for a modified Cassie–Baxter model of wetting on rough surfaces.

Acknowledgements

We would like to thank Prof. A. Derylo-Marczewska and Prof. L. Holysz and her co-workers from the Faculty of Chemistry, Marie Sklodowska Curie University, Lublin, Poland, for their kindness and help in synthesis and wettability measurements using KSV, Sigma700, Finland.

Funding

This work was supported by the Poland Operational Program 'Human Capital' [grant number PO KL.4.1.1] and National Science Centre [grant number DEC-2013/09/B/ST4/03711]; the US National Science Foundation [grant number CBET-1160151].

References

[1] T. Young, Philos. Trans. R. Soc. London **95**, 65 (1805).
[2] X.-M. Li, D. Reinhoudt, and M. Crego-Calama, Chem. Soc. Rev. **36**, 1350 (2007); D. Quéré, Annu. Rev. Mater. Sci. **38**, 71 (2008); D. Quéré and M. Reyssat, Philos. Trans. R. Soc. London, Ser. A **366**, 1539 (2008); M. Iino and Y. Fujimura, Appl. Phys. Lett. **94**, 261902 (2009); Z. Chu and S. Seeger, Chem. Soc. Rev. **43**, 2784 (2014).
[3] R.N. Wenzel, Ind. Eng. Chem. **28**, 988 (1936).
[4] A.B.D. Cassie and S. Baxter, Trans. Faraday Soc. **40**, 546 (1944).
[5] D. Quéré, Nat. Mater. **1**, 14 (2002).
[6] B. Bhushan, Philos. Trans. R. Soc. London, Ser. A **367**, 1445 (2009).
[7] M. Ye, X. Deng, J. Ally, P. Papadopoulos, F. Schellenberger, D. Vollmer, M. Kappl, and H.-J. Butt, Phys. Rev. Lett. **112**, 016101 (2014).
[8] C.G. Gray, K.E. Gubbins and C.G. Joslin, *Theory of Molecular Fluids 2: Applications* (Oxford University Press, Oxford, 2011), pp. 733–734, 914–916.
[9] R. Radhakrishnan, K.E. Gubbins, and M. Śliwinska-Bartkowiak, J. Chem. Phys. **112**, 1048 (2000); *ibid*. **116**, 1147 (2002).
[10] K.E. Gubbins, Y. Long, and M. Śliwinska-Bartkowiak, J. Chem. Thermodyn. **74**, 169 (2014).
[11] S.J. Gregg and K.S.W. Sing, *Adsorption, Surface Area and Porosity*, 2nd ed. (Academic Press, London, 1982), p. 128.
[12] A.W. Marczewski, A. Derylo-Marczewska, I. Skrzypek, S. Pikus, and M. Kozak, Adsorption **15**, 300 (2009).
[13] P. Bhange, D.S. Bhange, S. Pradhan, and V. Ramaswamy, Appl. Catal. A. **400**, 176 (2011).
[14] S.H. Joo, R. Ryoo, M. Kruk, and M. Jaroniec, J. Phys. Chem. B **106**, 4640 (2002).
[15] E.W. Washburn, Phys. Rev. Ser. 2 **17**, 273 (1921).
[16] B. Neirinck, J. van Deursen, O. Van der Biest, and J. Vleugels, J. Am. Ceram. Soc. **93**, 2515 (2010).
[17] W. Bigui, C. Qing, and Y. Caiyun, J. Colloid Interface Sci. **376**, 307 (2012).
[18] S. Kirdponpattara, M. Phisalaphong, and B. Zhang Newby, J. Colloid Interface Sci. **397**, 169 (2013).
[19] S. Lowell, J.E. Shields, M.A. Thomas, and M. Thommes, *Characterization of Porous Solids and Powders: Surface Area, Pore Size and Density* (Kluwer Academic Publishers, Dordrecht, 2004), Chap. 10.
[20] E.W. Washburn, Proc. Natl. Acad. Sci. U.S.A. **7**, 115 (1921).
[21] Y. Long, Ph. D. thesis, North Carolina State University, 2012.
[22] V. Kumar, S. Sridhar, and J.R. Errington, J. Chem. Phys. **135**, 184702 (2011).
[23] Q. Guo, Y. Liu, G. Jiang, and X. Zhang, Soft Matter **10**, 1182 (2014).